

## Article

# Experimentation and Numerical Modeling of Peak Temperature in the Weld Joint during Rotary Friction Welding of Dissimilar Plastic Rods

Chil-Chyuan Kuo <sup>1,2,3,\*</sup> , Naruboyana Gurumurthy <sup>1,4</sup>, Hong-Wei Chen <sup>1</sup> and Song-Hua Hunag <sup>5</sup>

<sup>1</sup> Department of Mechanical Engineering, Ming Chi University of Technology, No. 84, Gungjuan Road, New Taipei City 243, Taiwan

<sup>2</sup> Research Center for Intelligent Medical Devices, Ming Chi University of Technology, No. 84, Gungjuan Road, New Taipei City 243, Taiwan

<sup>3</sup> Department of Mechanical Engineering, Chang Gung University, No. 259, Wenhua 1st Road, Guishan District, Taoyuan City 33302, Taiwan

<sup>4</sup> Department of Mechanical Engineering, Presidency University, Rajankunte, Near Yelhanka, Bangalore 700073, India

<sup>5</sup> Li-Yin Technology Co., Ltd., No. 37, Lane 151, Section 1, Zhongxing Road, Wugu District, New Taipei City 241, Taiwan

\* Correspondence: jacksonk@mail.mcut.edu.tw

**Abstract:** Rotary friction welding (RFW) could result in lower welding temperature, energy consumption, or environmental effects as compared with fusion welding processes. RFW is a green manufacturing technology with little environmental pollution in the field of joining methods. Thus, RFW is widely employed to manufacture green products. In general, the welding quality of welded parts, such as tensile strength, bending strength, and surface hardness is affected by the peak temperature in the weld joint during the RFW of dissimilar plastic rods. However, hitherto little is known about the domain knowledge of RFW of acrylonitrile butadiene styrene (ABS) and polycarbonate (PC) polymer rods. To prevent random efforts and energy consumption, a green method to predict the peak temperature in the weld joint of dissimilar RFW of ABS and PC rods was proposed. The main objective of this work is to investigate the peak temperature in the weld joint during the RFW using COMSOL multiphysics software for establishing an empirical technical database of RFW of dissimilar polymer rods under different rotational speeds. The main findings include that the peak temperature affecting the mechanical properties of RFW of PC and ABS can be determined by the simulation model proposed in this work. The average error of predicting the peak temperature using COMSOL software for five different rotational speeds is about 15 °C. The mesh element count of 875,688 is the optimal number of meshes for predicting peak temperature in the weld joint. The bending strength of the welded part ( $y$ ) using peak welding temperature ( $x$ ) can be predicted by the equation of  $y = -0.019x^2 + 5.081x - 200.75$  with a correlation coefficient of 0.8857. The average shore A surface hardness, impact energy, and bending strength of the welded parts were found to be increased with increasing the rotational speed of RFW.

**Keywords:** energy consumption; environmental effects; rotary friction welding; acrylonitrile butadiene styrene; polycarbonate; peak temperature; weld joint; environmental pollution



**Citation:** Kuo, C.-C.; Gurumurthy, N.; Chen, H.-W.; Hunag, S.-H. Experimentation and Numerical Modeling of Peak Temperature in the Weld Joint during Rotary Friction Welding of Dissimilar Plastic Rods. *Polymers* **2023**, *15*, 2124. <https://doi.org/10.3390/polym15092124>

Academic Editor: Ammar Elsheikh

Received: 22 March 2023

Revised: 23 April 2023

Accepted: 26 April 2023

Published: 29 April 2023



**Copyright:** © 2023 by the authors. Licensee MDPI, Basel, Switzerland. This article is an open access article distributed under the terms and conditions of the Creative Commons Attribution (CC BY) license (<https://creativecommons.org/licenses/by/4.0/>).

## 1. Introduction

The energy consumption associated with the pre-processing, welding process, and post-processing steps of rotary friction welding (RFW) is obviously lower than gas metal arc welding. The advantage of adhesive bonding is that it can be bonded with dissimilar materials economically [1,2]. However, it is not suitable for industrial applications because of its low working efficiency. The RFW [3–7] is a solid-state joining process using a compressive axial force. According to practical experience in the industry, the RFW gives

many advantages. The welding process has a lower peak temperature in the weld joint than fusion welding (FW) [8,9]. Thus, intermetallic formation can be reduced. In addition, a wide range of dissimilar materials can be joined. The welding process does not need a filler metal and shielding gas. Many common defects associated with high-temperature melting and solidification during FW, such as solidification cracks or pores can be avoided. Therefore, welded parts with low defect rates as well as low distortion can be obtained easily. The material used and manufacturing costs are reduced greatly compared with subtractive techniques, such as machining from buck materials [10,11].

Zhang et al. [12] proposed a thermal compression bonding process to influence the friction flow of formation intermetallic compounds in friction welding. Results revealed that the frictional flow significantly promoted the formation of sub-micron-sized intermetallic compounds along the weld interface. Ma et al. [13] studied the effects of temperature on the mechanical performances of friction stir welded aluminum (Al) alloy joints. The results revealed that the pin increases heat input and material flow at the bottom, reducing the gradient along the thickness. Eliseev et al. [14] focused on the structural evolution in the transfer layer of Al alloy welds fabricated with various axial loads. It was found that the volume fraction and size of incoherent intermetallic particles decrease towards the center of the layer. Iftikhar et al. [15] investigate the friction stir spot welding of thermoplastic polymers. The results revealed that it is difficult to optimize the welding process parameters because of the dependence on many factors. Pereira et al. [16] focused on the influence of different welding methods on the mechanical strength of friction stir welds of thermoplastic polymers. The results revealed that the increase in the welding speed ratio increased the joint efficiency. Unfortunately, it was difficult to establish mathematical models because of the variation in welding conditions. Wang et al. [17] studied RFW on dissimilar brass bars using a pre-heating approach. It was found that a very narrow intermetallic compound layer was formed. Ishraq et al. [18] analyzed the weld strength by optimizing the process parameters of RFW at different levels. It was found that the reason for the high strength of a selected material is the optimal level of fiberglass. Hangai et al. [19] investigated the effects of the porosity of Al foam on the RFW. It was found that the Al foam can be welded to a polycarbonate plate by RFW. Dhooge et al. [20] proposed a promising welding approach for the fully automatic joining of pipelines, which is a new variant of the conventional friction welding process, and discussed the optimization of the duration of the friction phase.

Polymer is frequently used in some structures, such as automobiles, pressure vessels, and aircraft. Especially, the major difference between metal and polymer is that polymer is more lightweight and anti-corrosive than metal. Polycarbonate (PC) and acrylonitrile butadiene styrene (ABS) are compatible with each other since they have similar polarities. Therefore, mixtures of ABS and PC have been widely employed in engineering applications. In general, the major shortcomings of the trial-and-error method involve random efforts and energy consumption. It is well known that the [21–25] thermal analysis solutions can solve the most complex thermal challenges to predict the temperature. Unfortunately, hitherto little is known about the domain knowledge of the RFW of ABS and PC polymer rods. For this reason, the main objective of this study is to establish domain knowledge of the RFW of ABS and PC rods. To prevent random efforts and energy consumption, a green method to predict peak temperature in the weld joint of dissimilar RFW of ABS and PC rods was proposed. Therefore, the COMSOL multiphysics software [26] was employed to investigate the peak temperature in the weld joint during dissimilar RFW of ABS and PC rods. An infrared thermal imager was employed to investigate the peak temperature in the weld joint during RFW under five different rotational speeds. After RFW, the peak temperature obtained by the experiment was compared with the simulation results. Finally, an empirical technical database of RFW of dissimilar polymer rods under different rotational speeds is established.

## 2. Experimental Details

Figure 1 shows the research flowchart of this study. The research flow involves designing the workpiece, investigating optimum printing parameters using fused deposition modeling (FDM) [27], fabricating the workpieces, FRW, the determination of peak temperature by an infrared thermal imager [28] under five different rotational speeds [29], investigating the peak temperature by applying COMSOL multiphysics software, comparing the simulation results with the experimental results, and proposing a database of dissimilar RFW of ABS and PC rods. In the COMSOL multiphysics software, an attempt was made to simulate the peak temperature in the weld joint under the cycle time of 60 s. Generally, ABS thermoplastic material has good toughness and impact properties [30]. PC is an engineering thermoplastic material that has durability and thermal insulation [31,32]. In this study, two different kinds of filaments, i.e., ABS (Thunder 3D Inc., New Taipei City, Taiwan) and PC (Thunder 3D Inc., New Taipei City, Taiwan) were used to print welding workpieces.

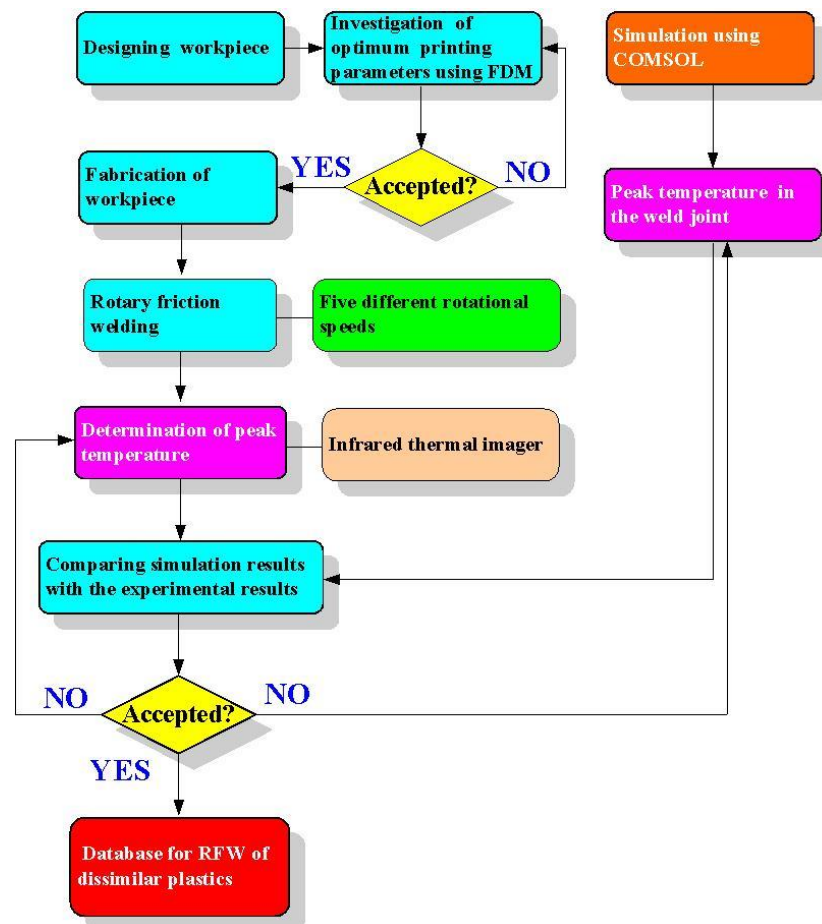
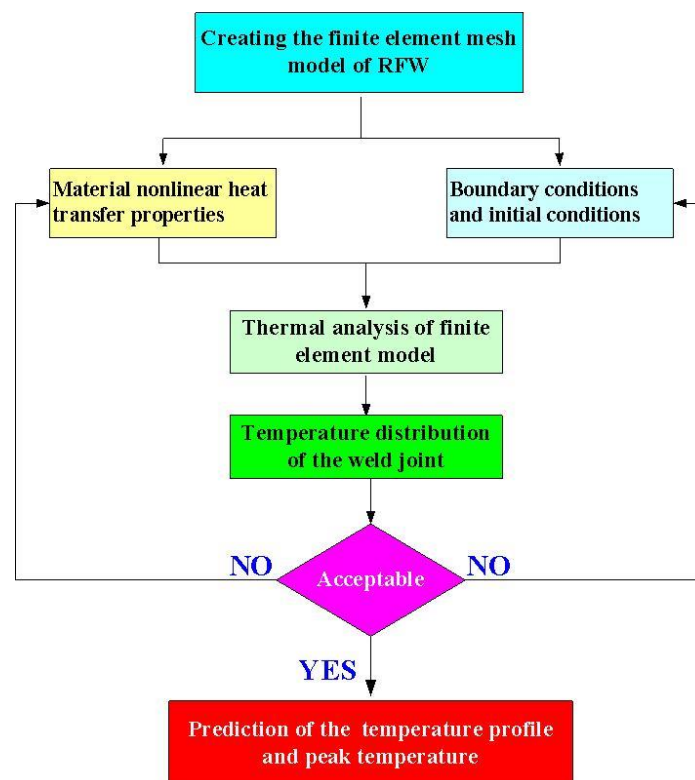


Figure 1. Research flowchart of this study.

Figure 2 shows the flowchart of numerical simulation by applying COMSOL multiphysics software, which includes the thermal pattern analysis and the suitable boundary conditions for the RFW model. The entire process involves establishing the finite element mesh model of RFW, setting the parameters for RFW, setting the material nonlinear heat transfer properties, setting both boundary conditions and initial conditions, thermal analysis of the finite element model, analysis of the temperature distribution of the weld joint, analysis of the temperature rise in the weld bead, and the prediction of the temperature profile and peak temperature. The welding workpiece is a cylindrical rod with a diameter of 20 mm and a length of 40 mm. The UltiMaker Cura software was then employed to

generate a printing program. The welding specimens were built with a fused deposition modeling (FDM) machine [33,34]. The build direction of the printed welding specimen was determined according to fewer supports, high dimensional accuracy, less printing time, and high surface quality. Firstly, the welding workpiece was designed using software named Cero (parametric technology corporation Inc., New Taipei City, Taiwan). According to practical experience, the printing parameters for PC welding workpieces involve a printing temperature of 245 °C, a printing speed of 50 mm/s, a layer thickness of 0.1 mm, and a printing bed temperature of 100 °C. In addition, the printing parameters for ABS welding workpieces involve a printing temperature of 230 °C, a printing speed of 45 mm/s, a layer thickness of 0.1 mm, and a printing bed temperature of 100 °C.



**Figure 2.** Flowchart of numerical simulation by applying COMSOL multiphysics software.

A conventional lathe was used to perform RFW. In general, the RFW provides axial movement to obtain the required weld strength. During RFW, one welding specimen was rotated at a constant speed while the other was held stationary. Two welding specimens were brought together under pressure for a certain period of time. In this study, the cycle time of FW was set to 60 s. The cycle time involves a friction time of 30 s, a weld time of 20 s, and a cooling time of 10 s. The burn-off length was set to 2 mm since the FW was carried out 20 times with a weld length of 0.1 mm each time. The selection of five rotational speeds is mainly based on the specifications of the lathe used in this study. To investigate the effects of rotational speed on peak temperature in the weld joint, five different rotational speeds, i.e., 330 rpm, 490 rpm, 650 rpm, 950 rpm, and 1350 rpm were carried out in this study. The peak temperature in the weld joint during the RFW of dissimilar specimens was monitored and recorded using an infrared camera (BI-TM-F01P, Panrico trading Inc., New Taipei City, Taiwan). After RFW, the shore A surface hardness test (MET-HG-A, SEAT Inc. New Taipei City, Taiwan), three-point bending test (RH-30, Shimadzu Inc., Kyoto, Japan), and impact test (780, Instron Inc., Massachusetts, MA, USA) were carried out to evaluate the mechanical properties of the frictionally welded parts.

### 3. Results and Discussion

In general, the welding quality of the welded parts was influenced by the peak temperature in the weld joint during RFW of dissimilar plastic rods since the mechanical properties were affected by the peak temperature during RFW [35]. In this study, the COMSOL multiphysics software was used to investigate the peak temperature in the weld joint. Ten different kinds of element sizes, i.e., 0.4 mm, 0.5 mm, 0.6 mm, 0.7 mm, 0.8 mm, 0.9 mm, 1.0 mm, 1.1 mm, 1.2 mm, and 1.3 mm were performed to investigate the peak temperature in the weld joint during RFW. Figure 3 shows the geometry and mesh of the workpieces in the simulation. The element size of the processed workpieces is 0.8 mm. To determine the type of mesh suitable for RFW, Figure 4 describes the number of meshes as a function of computing time and peak temperature in the weld joint. As can be seen, a higher number of meshes has a higher computation time. In addition, calculating the peak temperature in the weld joint during RFW of dissimilar plastic rods by applying COMSOL multiphysics software was feasible [36]. Especially, the peak temperature predicted by the COMSOL multiphysics software using a mesh element count of 875,688 is very close to that obtained by the experimental result. This means that the mesh element count of 875,688 seems to be the optimal number of meshes for predicting peak temperature in the weld joint. Figure 5 shows the temperature distributions for RFW of two dissimilar workpieces. The thermal model takes into account various parameters such as friction pressure, rotational speed, feed rate, and material properties of the polymer rods being joined. As can be seen, the temperature distribution, amount of energy required to achieve a successful weld, and heat-affected zone can be calculated based on the thermal model in the COMSOL multiphysics software. Figure 6 shows the peak temperature in the weld joint for five different rotational speeds predicted by COMSOL multiphysics software. The peak temperatures in the weld joint for five different rotational speeds of 330 rpm, 490 rpm, 650 rpm, 950 rpm, and 1350 rpm are 53 °C, 70 °C, 86 °C, 116 °C, and 156 °C, respectively.

To investigate the repeatability of the RFW experiments in this study, three samples were used in this study. The material emissivity of ABS and PC is about 0.92 and 0.95, respectively. The image resolution for the thermal imaging data is about  $1440 \times 1080$  pixels. In general, the melting temperature for PC and ABS is about  $155 \pm 10$  °C and  $245 \pm 10$  °C, respectively [37,38]. Figure 7 shows the relationship between weld joint temperature and FW time for PLA and PLA rods at a rotational speed of 950 rpm. As can be seen, the relationship between weld time and joint temperature for the RFW of ABS and PC workpieces at a rotational speed of 950 rpm is repeatable. The peak temperature in the weld joint was found to be approximately 118 °C. This result is supported by the experiment proposed by Mura et al. [39], showing the glass transition temperature of PC-ABS is approximately 125 °C. Figure 8 shows the relationship between weld joint temperature and FW time for PLA and PLA rods at five different rotational speeds. The results showed that the average peak temperatures of weld joint for rotational speeds of 330 rpm, 490 rpm, 650 rpm, 950 rpm, and 1350 rpm are approximately 88 °C, 99 °C, 106 °C, 114 °C, and 153 °C, respectively. The results revealed that the peak temperatures in the weld joint increase gradually with increasing rotational speed.

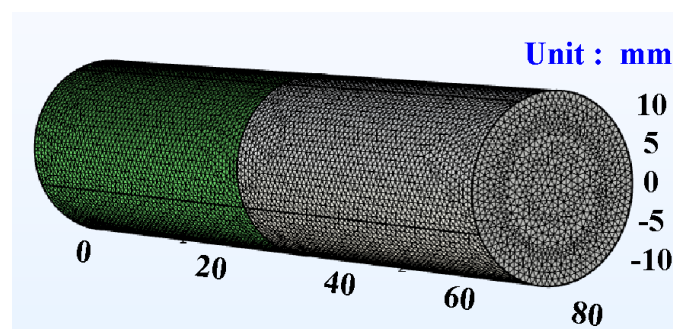


Figure 3. Geometry and mesh of the workpieces in the simulation for the element size of 0.8 mm.

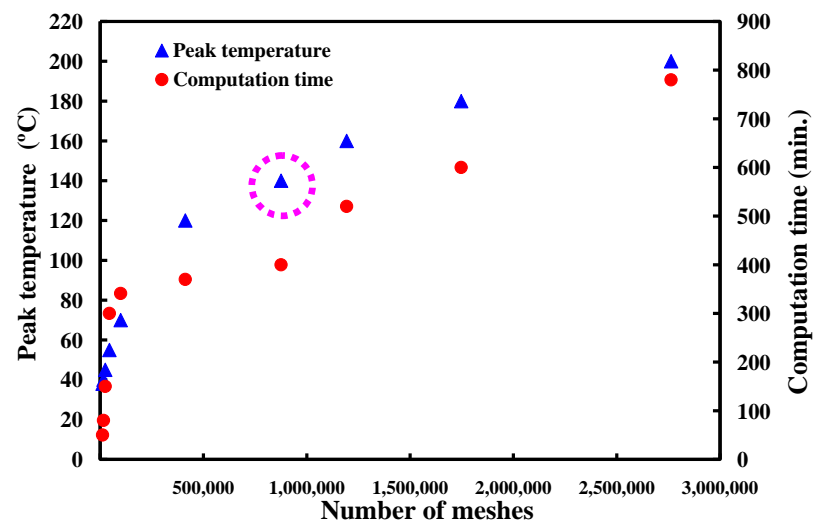


Figure 4. Number of meshes as a function of computing time and peak temperature in the weld joint.

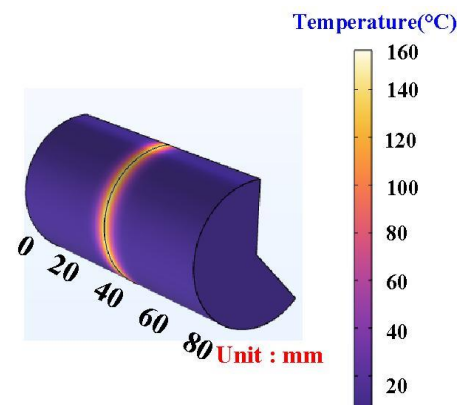


Figure 5. Temperature distributions for RFW of two dissimilar workpieces.

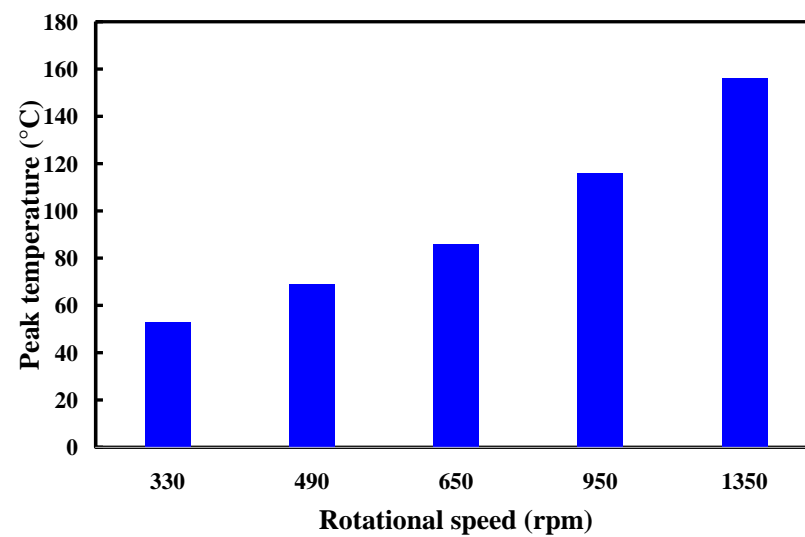


Figure 6. Peak temperature in the weld joint for five different rotational speeds predicted by COMSOL multiphysics software.

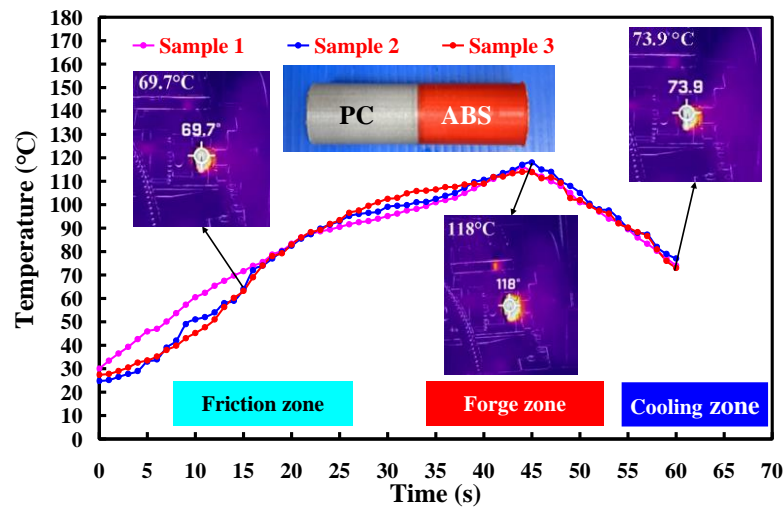


Figure 7. Temperature history in the weld joint for RFW of PC and ABS rods at a rotational speed of 950 rpm.

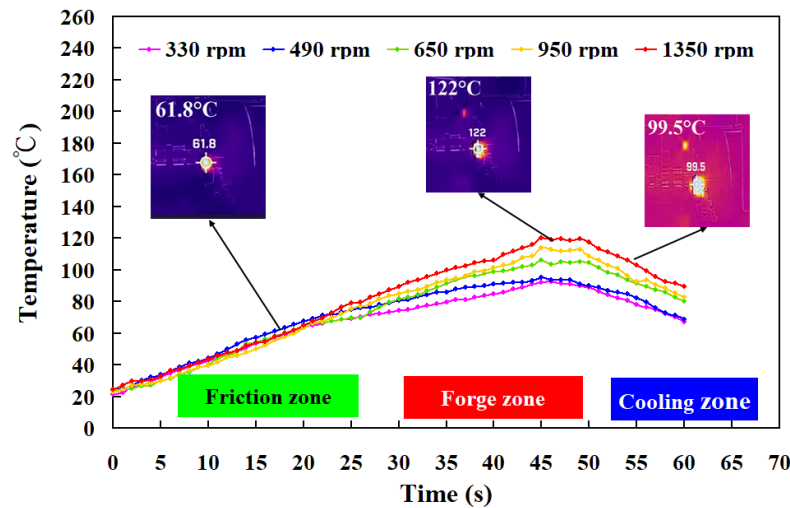


Figure 8. Temperature history in the weld joint for RFW of PC and ABS rods at five different rotational speeds.

Figure 9 shows the surface hardness in the weld joint for RFW of PC and ABS rods at five different rotational speeds. As can be seen, the average shore A surface hardness in the weld joint is increased with increasing the rotational speed of RFW. Figure 10 shows the impact energy of dissimilar polymer rods welded at five different rotational speeds. The results showed that the impact energy in the weld joint is increased with increasing the rotational speed of RFW. This result was also confirmed by the experiment proposed by Dhaiwat et al. [40]. Figure 11 shows the ending strength of the welded part under five different rotational speeds. As can be seen, the bending strength in the weld joint is increased with increasing the rotational speed of RFW. Figure 12 shows the bending strength as a function of peak welding temperature. It was found that the equation of  $y = -0.019x^2 + 5.081x - 200.75$  with the correlation coefficient [41] of 0.8857 seems to be an optimum trend equation for predicting the bending strength of the welded part (y) using peak welding temperature (x).

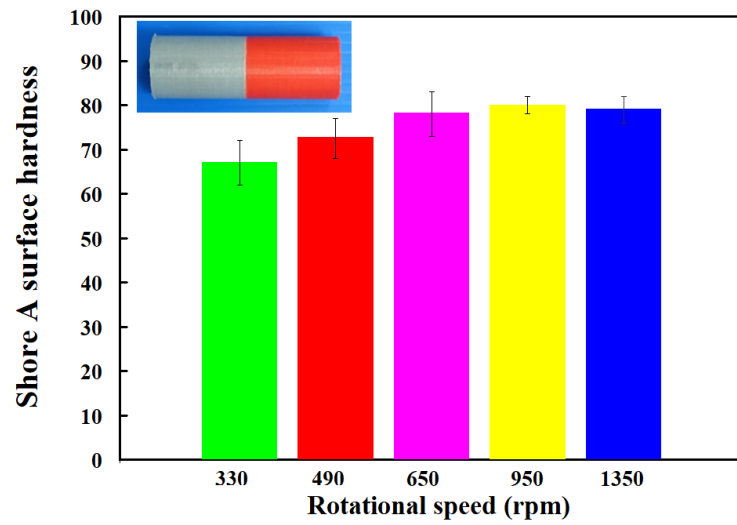


Figure 9. Surface hardness in the weld joint for RFW of PC and ABS rods at five different rotational speeds.

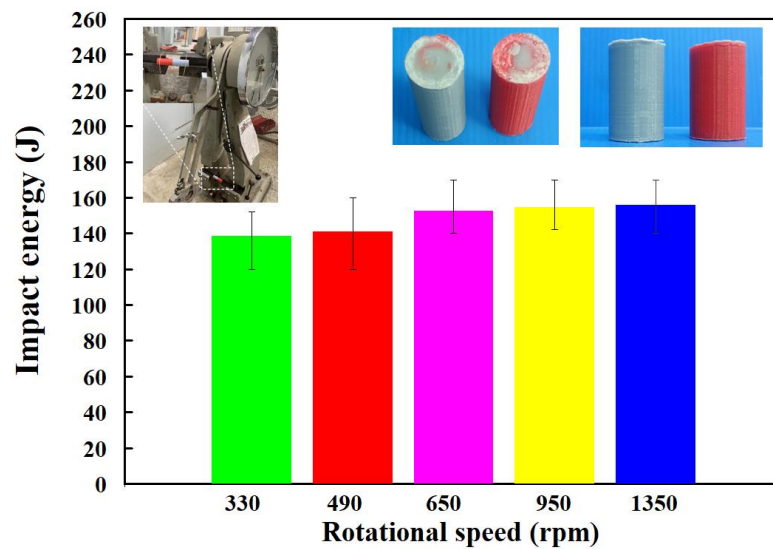


Figure 10. Impact energy of dissimilar polymer rods welded by five different rotational speeds.

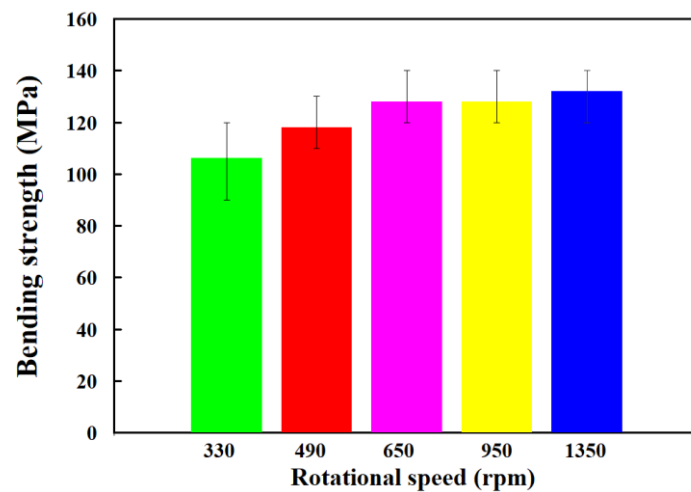


Figure 11. Bending strength of the welded part under five different rotational speeds.

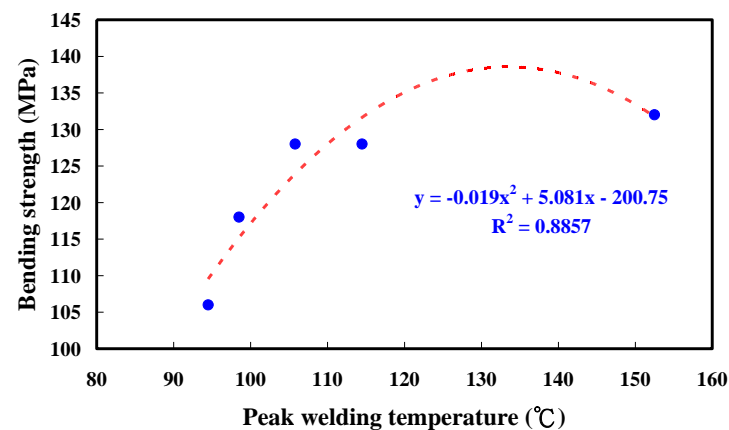


Figure 12. Bending strength as a function of peak welding temperature.

Figure 13 shows the comparison of the numerical simulation and experimental results of the peak temperature for RFW of PC and ABS rods at five different rotational speeds. Figure 14 shows the comparison of the numerical simulation and experimental results of the temperature profile. As can be seen, the difference in the peak temperature between simulation and experimental results for rotational speeds of 330 rpm, 490 rpm, 650 rpm, 950 rpm, and 1350 rpm is about 34 °C, 29 °C, 20 °C, −2 °C, and −3 °C, respectively. Thus, the average error of predicting the peak temperature by applying COMSOL software for five different rotational speeds is about 15 °C.

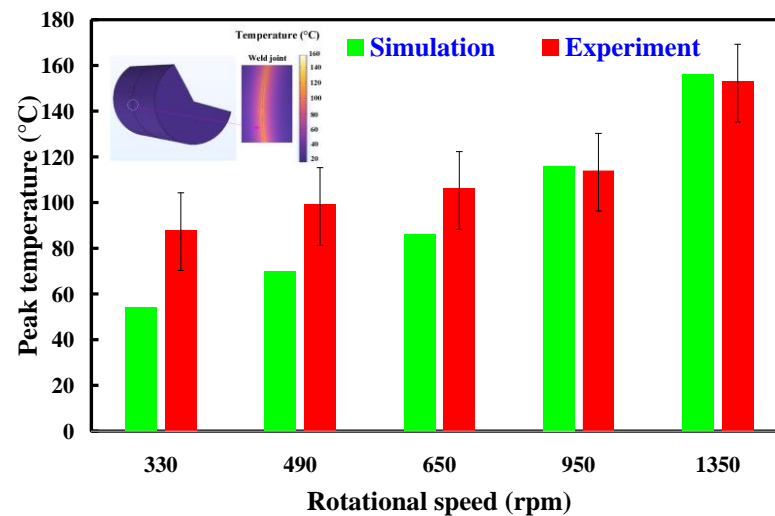
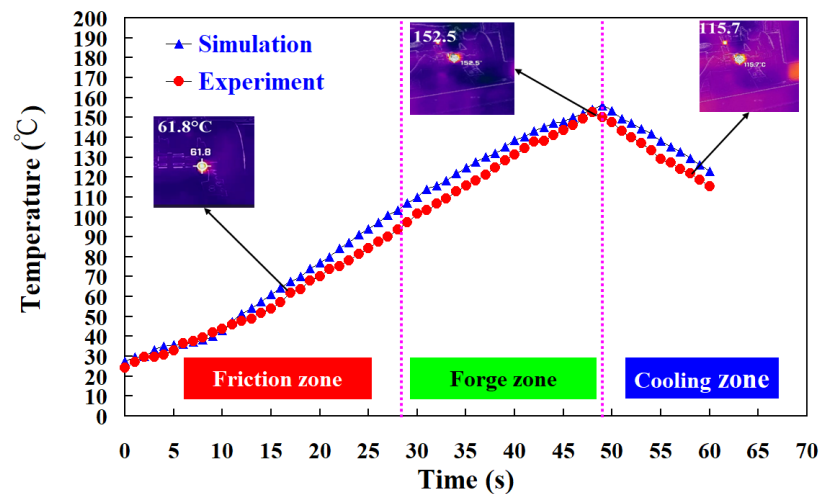


Figure 13. Comparison of the numerical simulation and experimental results of the peak temperature for RFW of PC and ABS rods at five different rotational speeds.

In practice, one of the advantages of the FRW is reduced energy consumption as compared to arc welding processes [42]. Therefore, the RFW of dissimilar polymer rods is a green manufacturing technique for joining dissimilar polymer rods and meets sustainable development (SDGs 9 and 12) [43]. In general, this technique can be used for joining automotive components, aircraft components, axle shafts, aerospace components, fluid mechanical components, or transmission shafts [44,45]. In this study, a conventional lathe was employed to perform RFW of ABS and PC rods. In future investigations, the computer numerical control turning machine [46] is recommended to perform RFW of ABS and PC rods since the feed rate of RFW can be precisely controlled to replace human error. In addition, the rotational speed [47–52] can be changed during the whole process of RFW. These topics are interesting research topics and are currently being investigated, and the results will be presented in later works.



**Figure 14.** Comparison of the numerical simulation and experimental results of the temperature profile.

#### 4. Conclusions

An energy-related key performance indicator is frequently used as a tool to evaluate the energy consumption of manufacturing processes, focusing on energy consumption and environmental impact. RFW is a green manufacturing process and is becoming useful in lots of industrial applications. RFW is a sustainable manufacturing technology with low energy consumption since it generates heat through mechanical friction between thermoplastics. The advantages of RFW include being free from thermal distortion or porosity which are defects seen in other welding techniques. In this work, an analysis of the peak temperature in the weld joint during dissimilar RFW of ABS and PC rods by applying the COMSOL multiphysics software is presented. The main conclusions from the experimental work in this study are as follows:

1. The use of COMSOL software was feasible for calculating the peak temperature in the weld joint during dissimilar RFW of ABS and PC rods. The mesh element count of 875,688 is the optimal number of meshes for predicting peak temperature in the weld joint. The average error of predicting the peak temperature using the COMSOL software for five different rotational speeds is about 15 °C.
2. The bending strength of the welded part ( $y$ ) using peak welding temperature ( $x$ ) can be predicted by the equation of  $y = -0.019x^2 + 5.081x - 200.75$  with the correlation coefficient with a correlation coefficient of 0.8857.
3. The bending strength, average shore A surface hardness, and impact energy of the welded parts were increased with increasing the rotational speed of RFW.

**Author Contributions:** C.-C.K.: Wrote the paper, conceived and designed the analysis, and performed the analysis. N.G., H.-W.C. and S.-H.H.: Collected the data and contributed data or analysis tools. All authors have read and agreed to the published version of the manuscript.

**Funding:** This study received financial support from the Ministry of Science and Technology of Taiwan under contract nos. NSTC 111-2221-E-131-015-MY2, MOST 110-2221-E-131-023 and MOST 109-2637-E-131-004.

**Institutional Review Board Statement:** Not applicable.

**Data Availability Statement:** Data and materials are available.

**Conflicts of Interest:** The authors declare no conflict of interest.

## References

1. Wang, S.; Liang, W.; Duan, L.; Li, G.; Cui, J. Effects of loading rates on mechanical property and failure behavior of single-lap adhesive joints with carbon fiber reinforced plastics and aluminum alloys. *Int. J. Adv. Manuf. Technol.* **2020**, *106*, 2569–2581. [[CrossRef](#)]
2. Hamed, H.; Kamyabi-Gol, A. A novel approach to modelling the bond characteristics between CFRP fabrics and steel plate joints under quasi-static tensile loads. *Int. J. Adv. Manuf. Technol.* **2021**, *116*, 3247–3261. [[CrossRef](#)]
3. Yin, P.; Xu, C.; Pan, Q.; Zhang, W.; Jiang, X. Effect of Different Ultrasonic Power on the Properties of RHA Steel Welded Joints. *Materials* **2022**, *15*, 768. [[CrossRef](#)] [[PubMed](#)]
4. Li, B.; Liu, Q.; Jia, S.; Ren, Y.; Yang, P. Effect of V Content and Heat Input on HAZ Softening of Deep-Sea Pipeline Steel. *Materials* **2022**, *15*, 794. [[CrossRef](#)] [[PubMed](#)]
5. Lambiase, F.; Grossi, V.; Paoletti, A. Effect of tilt angle in FSW of polycarbonate sheets in butt configuration. *Int. J. Adv. Manuf. Technol.* **2020**, *107*, 489–501. [[CrossRef](#)]
6. Delijaicov, S.; Rodrigues, M.; Farias, A.; Neves, M.D.; Bortolussi, R.; Miyazaki, M.; Brandão, F. Microhardness and residual stress of dissimilar and thick aluminum plates AA7181-T7651 and AA7475-T7351 using bobbin, top, bottom, and double-sided FSW methods. *Int. J. Adv. Manuf. Technol.* **2020**, *108*, 277–287. [[CrossRef](#)]
7. Hassan, A.J.; Boukharouba, T.; Miroud, D. Concept of forge application under effect of friction time for AISI 316 using friction welding process. *Int. J. Adv. Manuf. Technol.* **2021**, *112*, 2223–2231. [[CrossRef](#)]
8. Le, J.; Zhang, H.; Le, M.; Hu, L. Research on identification of the corner point of 90° weld based on multi-sensor signal fusion technology. *Int. J. Adv. Manuf. Technol.* **2020**, *107*, 2277–2290. [[CrossRef](#)]
9. Zhang, B.; Shi, Y.; Cui, Y.; Wang, Z.; Chen, X. A high-dynamic-range visual sensing method for feature extraction of welding pool based on adaptive image fusion. *Int. J. Adv. Manuf. Technol.* **2021**, *117*, 1675–1687. [[CrossRef](#)]
10. Wu, D.; Wang, H.; Yu, J. Research on machining error transmission mechanism and compensation method for near-net-shaped jet engine blades CNC machining process. *Int. J. Adv. Manuf. Technol.* **2021**, *117*, 2755–2773. [[CrossRef](#)]
11. Equbal, A.; Equbal, M.A.; Equbal, M.I.; Ravindrannair, P.; Khan, Z.A.; Badruddin, I.A.; Kamangar, S.; Tirth, V.; Javed, S.; Kittur, M.I. Evaluating CNC Milling Performance for Machining AISI 316 Stainless Steel with Carbide Cutting Tool Insert. *Materials* **2022**, *15*, 8051. [[CrossRef](#)] [[PubMed](#)]
12. Zhang, D.; Qin, G.; Geng, P.; Ma, H. Study of plastic flow on intermetallic compounds formation in friction welding of aluminum alloy to stainless steel. *J. Manuf. Process.* **2021**, *64*, 20–29. [[CrossRef](#)]
13. Ma, X.; Xu, S.; Wang, F.; Zhao, Y.; Meng, X.; Xie, Y.; Wan, L.; Huang, Y. Effect of Temperature and Material Flow Gradients on Mechanical Performances of Friction Stir Welded AA6082-T6 Joints. *Materials* **2022**, *15*, 6579. [[CrossRef](#)] [[PubMed](#)]
14. Eliseev, A.; Osipovich, K.; Fortuna, S. Gradient Structure of the Transfer Layer in Friction Stir Welding Joints. *Materials* **2022**, *15*, 6772. [[CrossRef](#)]
15. Iftikhar, S.H.; Mourad, A.-H.I.; Sheikh-Ahmad, J.; Almaskari, F.; Vincent, S. A Comprehensive Review on Optimal Welding Conditions for Friction Stir Welding of Thermoplastic Polymers and Their Composites. *Polymers* **2021**, *13*, 1208. [[CrossRef](#)] [[PubMed](#)]
16. Pereira, M.A.R.; Amaro, A.M.; Reis, P.N.B.; Loureiro, A. Effect of Friction Stir Welding Techniques and Parameters on Polymers Joint Efficiency—A Critical Review. *Polymers* **2021**, *13*, 2056. [[CrossRef](#)] [[PubMed](#)]
17. Wang, G.L.; Li, J.L.; Wang, W.L.; Xiong, J.T.; Zhang, F.S. Rotary friction welding on dissimilar metals of aluminum and brass by using pre-heating method. *Int. J. Adv. Manuf. Technol.* **2018**, *99*, 1293–1300. [[CrossRef](#)]
18. Ishraq, M.Y.; Maqsood, S.; Naeem, K.; Abid, M.; Omair, M. Analysing significant process parameters for friction stir welding of polymer composite. *Int. J. Adv. Manuf. Technol.* **2019**, *105*, 4973–4987. [[CrossRef](#)]
19. Hangai, Y.; Omika, K.; Inoue, M.; Kitamura, A.; Mitsugi, H.; Fujii, H.; Kamakoshi, Y. Effect of porosity of aluminum foam on welding between aluminum foam and polycarbonate plate during friction welding. *Int. J. Adv. Manuf. Technol.* **2022**, *120*, 1071–1078. [[CrossRef](#)]
20. Faes, K.; Dhooge, A.; De Baets, P.; Afschrift, P. New friction welding process for pipeline girth welds—Welding time optimisation. *Int. J. Adv. Manuf. Technol.* **2009**, *43*, 982–992. [[CrossRef](#)]
21. Chang, Q.; Gao, P.; Zhang, J.; Huo, Y.; Zhang, Z.; Xie, J. Numerical Simulation of Copper-Aluminum Composite Plate Casting and Rolling Process and Composite Mechanism. *Materials* **2022**, *15*, 8139. [[CrossRef](#)] [[PubMed](#)]
22. Bochenek, B.; Tajs-Zielińska, K. Cellular Automaton Mimicking Colliding Bodies for Topology Optimization. *Materials* **2022**, *15*, 8057. [[CrossRef](#)]
23. Sun, C.; Zhong, C.; Wang, L.; Qin, L. Design and Preparation of Double-Harmonic Piezoelectric Composite Lamination. *Materials* **2022**, *15*, 7959. [[CrossRef](#)] [[PubMed](#)]
24. Yang, N.; Gong, Y.; He, P.; Zhou, C.; Zhou, R.; Shao, H.; Chen, G.; Lin, X.; Bie, H. Influence of Circular through Hole in Pt-Rh Bushing on Temperature Propagation at High Temperature. *Materials* **2022**, *15*, 7832. [[CrossRef](#)] [[PubMed](#)]
25. Deng, X.; Li, J.; Xie, X. Effect of Preheating Temperature on Thermal-Mechanical Properties of Dry Vibrating MgO-Based Material Lining in the Tundish. *Materials* **2022**, *15*, 7699. [[CrossRef](#)] [[PubMed](#)]
26. Jiang, J.; Chen, Q.; Hu, S.; Shi, Y.; He, Z.; Huang, Y.; Hui, C.; Chen, Y.; Wu, H.; Lu, G. Effect of Electro-Thermo-Mechanical Coupling Stress on Top-Cooled E-Mode AlGaN/GaN HEMT. *Materials* **2023**, *16*, 1484. [[CrossRef](#)]
27. Nasir, M.H.M.; Taha, M.M.; Razali, N.; Ilyas, R.A.; Knight, V.F.; Norrrahim, M.N.F. Effect of Chemical Treatment of Sugar Palm Fibre on Rheological and Thermal Properties of the PLA Composites Filament for FDM 3D Printing. *Materials* **2022**, *15*, 8082. [[CrossRef](#)]

28. Haider, S.M.; Khan, S.A.; Ali, M.A.; Farooq, M.U.; Ishfaq, K. Thermal experiments and analysis on adhesive cleaning of work-holding devices by grinding. *Int. J. Adv. Manuf. Technol.* **2022**, *122*, 3849–3865. [[CrossRef](#)]
29. Kuo, C.-C.; Chen, H.-W.; Xu, J.-Y.; Lee, C.-H.; Hunag, S.-H. Effects of Rotational Speed on Joint Characteristics of Green Joining Technique of Dissimilar Polymeric Rods Fabricated by Additive Manufacturing Technology. *Polymers* **2022**, *14*, 4822. [[CrossRef](#)]
30. Maier, R.; Istrate, A.M.; Despa, A.; Mandoc, A.C.; Bucaciuc, S.; Stoica, R. Investigation into Thermomechanical Response of Polymer Composite Materials Produced through Additive Manufacturing Technologies. *Materials* **2022**, *15*, 5069. [[CrossRef](#)]
31. König, S.; Kreis, P.; Herbert, C.; Wego, A.; Steinmann, M.; Wang, D.; Frank, E.; Buchmeiser, M.R. Melt-Spinning of an Intrinsically Flame-Retardant Polyacrylonitrile Copolymer. *Materials* **2020**, *13*, 4826. [[CrossRef](#)]
32. Rajagopalan, S.R.; Lee, B.-Y.; Kang, S.-T. Prediction of the Rheological Properties of Fresh Cementitious Suspensions Considering Microstructural Parameters. *Materials* **2022**, *15*, 7044. [[CrossRef](#)]
33. Challa, B.T.; Gummadi, S.K.; Elhattab, K.; Ahlstrom, J.; Sikder, P. In-house processing of 3D printable polyetheretherketone (PEEK) filaments and the effect of fused deposition modeling parameters on 3D-printed PEEK structures. *Int. J. Adv. Manuf. Technol.* **2022**, *121*, 1675–1688. [[CrossRef](#)]
34. Zhu, Q.; Yu, K.; Li, H.; Zhang, Q.; Tu, D. Rapid residual stress prediction and feedback control during fused deposition modeling of PLA. *Int. J. Adv. Manuf. Technol.* **2022**, *118*, 3229–3240. [[CrossRef](#)]
35. He, X.; Li, L.; He, X.; Xie, C. Multi-Physical Field Simulation of Cracking during Crystal Growth by Bridgman Method. *Materials* **2023**, *16*, 3260. [[CrossRef](#)] [[PubMed](#)]
36. Yang, F.; Zhang, J.; Guo, C.A.; Zhao, S. Investigation of electrochemical machining for gradual change special-shaped deep spiral hole based on COMSOL. *Int. J. Adv. Manuf. Technol.* **2020**, *108*, 2717–2725. [[CrossRef](#)]
37. Reich, M.J.; Woern, A.L.; Tanikella, N.G.; Pearce, J.M. Mechanical Properties and Applications of Recycled Polycarbonate Particle Material Extrusion-Based Additive Manufacturing. *Materials* **2019**, *12*, 1642. [[CrossRef](#)]
38. Chua, B.-L.; Baek, S.-H.; Park, K.; Ahn, D.-G. Numerical Investigation of Deposition Characteristics of PLA on an ABS Plate Using a Material Extrusion Process. *Materials* **2021**, *14*, 3404. [[CrossRef](#)] [[PubMed](#)]
39. Mura, A.; Ricci, A.; Canavese, G. Investigation of Fatigue Behavior of ABS and PC-ABS Polymers at Different Temperatures. *Materials* **2018**, *11*, 1818. [[CrossRef](#)]
40. Trivedi, D.N.; Rachchh, N.V. Graphene and its application in thermoplastic polymers as nano-filler—A review. *Polymer* **2022**, *240*, 124486. [[CrossRef](#)]
41. Qi, M.; Cao, L.; Zhao, Y.; Jia, F.; Song, S.; He, X.; Yan, X.; Huang, L.; Yin, Z. Quantitative Analysis of Mixed Minerals with Finite Phase Using Thermal Infrared Hyperspectral Technology. *Materials* **2023**, *16*, 2743. [[CrossRef](#)] [[PubMed](#)]
42. Shrivastava, A.; Krones, M.; Pfefferkorn, F.E. Comparison of energy consumption and environmental impact of friction stir welding and gas metal arc welding for aluminum. *CIRP J. Manuf. Sci. Technol.* **2015**, *9*, 159–168. [[CrossRef](#)]
43. Li, K.; Zhou, T.; Liu, B.H. Internet-based intelligent and sustainable manufacturing: Developments and challenges. *Int. J. Adv. Manuf. Technol.* **2020**, *108*, 1767–1791. [[CrossRef](#)]
44. Belkahla, Y.; Mazouzi, A.; Lebouachera, S.E.I.; Hassan, A.J.; Fides, M.; Hvizdoš, P.; Cheniti, B.; Miroud, D. Rotary friction welded C45 to 16NiCr6 steel rods: Statistical optimization coupled to mechanical and microstructure approaches. *Int. J. Adv. Manuf. Technol.* **2021**, *116*, 2285–2298. [[CrossRef](#)]
45. Barrionuevo, G.O.; Mullo, J.L.; Ramos-Grez, J.A. Predicting the ultimate tensile strength of AISI 1045 steel and 2017-T4 aluminum alloy joints in a laser-assisted rotary friction welding process using machine learning: A comparison with response surface methodology. *Int. J. Adv. Manuf. Technol.* **2021**, *116*, 1247–1257. [[CrossRef](#)]
46. Esangbedo, M.O.; Abifarin, J.K. Cost and Quality Optimization Taguchi Design with Grey Relational Analysis of Halloysite Nanotube Hybrid Composite: CNC Machine Manufacturing. *Materials* **2022**, *15*, 8154. [[CrossRef](#)]
47. Bouarroudj Eo Abdi, S.; Miroud, D. Improved performance of a heterogeneous weld joint of copper-steel AISI 1045 obtained by rotary friction using a metal powder insert. *Int. J. Adv. Manuf. Technol.* **2023**, *124*, 1905–1924. [[CrossRef](#)]
48. Szwajka, K.; Zielińska-Szwajka, J.; Trzepieciński, T. Microstructure and Mechanical Properties of Solid-State Rotary Friction Welded Inconel 713C and 32CrMo4 Steel Joints Used in a Turbocharger Rotor. *Materials* **2023**, *16*, 2273. [[CrossRef](#)]
49. Insua, P.; Nakkiew, W.; Wisittipanich, W. Post Weld Heat Treatment Optimization of Dissimilar Friction Stir Welded AA2024-T3 and AA7075-T651 Using Machine Learning and Metaheuristics. *Materials* **2023**, *16*, 2081. [[CrossRef](#)]
50. Ahmed, M.M.Z.; Essa, A.R.S.; Ataya, S.; El-Sayed Seleman, M.M.; El-Aty, A.A.; Alzahrani, B.; Touileb, K.; Bakkar, A.; Ponnore, J.J.; Mohamed, A.Y.A. Friction Stir Welding of AA5754-H24: Impact of Tool Pin Eccentricity and Welding Speed on Grain Structure, Crystallographic Texture, and Mechanical Properties. *Materials* **2023**, *16*, 2031. [[CrossRef](#)]
51. Pang, Z.; Yang, J.; Cai, Y. Effects of Rotational Speed on the Microstructure and Mechanical Properties of 2198-T8 Al-Li Alloy Processed by Friction Spot Welding. *Materials* **2023**, *16*, 1807. [[CrossRef](#)] [[PubMed](#)]
52. Dong, J.; Huang, Y.; Zhu, J.; Guan, W.; Yang, L.; Cui, L. Variation Mechanism of Three-Dimensional Force and Force-Based Defect Detection in Friction Stir Welding of Aluminum Alloys. *Materials* **2023**, *16*, 1312. [[CrossRef](#)] [[PubMed](#)]

**Disclaimer/Publisher’s Note:** The statements, opinions and data contained in all publications are solely those of the individual author(s) and contributor(s) and not of MDPI and/or the editor(s). MDPI and/or the editor(s) disclaim responsibility for any injury to people or property resulting from any ideas, methods, instructions or products referred to in the content.